REAL IMAGE DEHAZING BASED ON MODEL OPTIMIZATION AND LUMINANCE ENHANCEMENT

Lingyu LI[1], Zhiyong TAO[1, *], Sen LIN[2]

Addressing the issues of blurred details, color distortion, and reduced brightness in hazy images, we propose a dehazing method grounded in model optimization and brightness enhancement. Firstly, the traditional atmospheric scattering model is optimized based on the dark channel prior theory. Second, a luminance augmentation branch is proposed to improve the image brightness. Finally, the images processed by both the model optimization and luminance enhancement branches are fused and subsequently color-corrected to enhance the visual quality of the images. Experimental results on the RESIDE dataset and real-world images show that our method outperforms classical and the latest dehazing methods.

Keywords: Dehazing method, Atmospheric scattering model, Model optimization, Luminance enhancement

1. Introduction

Images captured in hazy weather suffer from detail loss and contrast reduction, limiting their application in advanced vision areas like target recognition[1], tracking, satellite remote sensing monitoring[2], and automatic driving[3]. Image dehazing techniques mitigate the haze effect, enhancing image clarity and naturalness, and facilitating observation and analysis. Consequently, designing an effective image dehaze method is of great research significance.

Currently, methods for image dehazing are divided into three main categories: image enhancement methods, image restoration methods, and deep learning methods. Dehaze methods based on image enhancement mainly focus on enhancing the contrast and color saturation of the image without considering the principle of haze formation and the essential cause of image degradation. Histogram Equalisation is a crucial technique used for image enhancement to improve the contrast of an image. However, the method may enhance noise and introduce unnatural effects. Therefore, Liu et al. [4] provided a simple but effective method for contrast enhancement-Colour-Preserving AHE(CP-AHE).

[1] School of Electronic and Information Engineering, Liaoning Technical University, Huludao, Liaoning, 125105, China, e-mail: lly1341615837@163.com
[2] School of Automation and Electrical Engineering, Shenyang Ligong University, Shenyang, Liaoning, 110159, China, e-mail: lin_sen6@126.com
* Corresponding author: Zhiyong TAO, e-mail: taozhiyong@lntu.edu.cn

This novel approach can effectively maintain the color of the dehazed image. The image restoration-based dehazing method mainly starts from the cause of image degradation itself, constructs a physical model for fog image imaging, estimates the parameters in the model, and obtains a clear haze-free image by inversely solving the formula. He et al. [5] proposed the Dark Channel Prior (DCP) theory. Subsequently, He et al. [6] proposed a method to optimize the transmittance using guided filtering. In addition, Ju et al. [7] designed an Enhanced ASM (EASM), which effectively solves the problem of the dark image after dehazing processing. Ling et al. [8] proposed Saturation Line Prior (SLP) by observing many haze-free images and a new SLP-based dehazing framework is proposed. In recent years, deep learning-based dehazing methods have made significant progress. Cai et al. [9] proposed an end-to-end dehazing system, Dehaze-Net, the most representative deep learning dehazing network in the early days. Dong et al. [10] proposed a multi-scale enhancement dehazing network (MSBDN) with dense feature fusion based on U-Net architecture, which gradually recovers haze-free images by developing a simple and effective enhancement decoder [11]. Inspired by meta-learning, Jia et al. [12] proposed a novel meta-attention dehazing network (MADN) to recover clear images directly from haze images without using a physical scattering model.

Considering that the performance of deep learning-based dehazing methods is limited by the diversity of training datasets, the design of network structures lacks theoretical support, and the issues of poor dehazing effects, detail loss, and image distortion in image enhancement and restoration-based dehazing methods remain to be addressed, we propose an image dehazing method based on model optimization and luminance enhancement.

Our contributions are:

(1) Optimizing the atmospheric scattering model and combining the quadtree search and gradient-domain guided filtering algorithms to mitigate image distortion from inaccurate parameter estimation.

(2) Aiming at the overall darkness of the image processed by the dehazing method based on the atmospheric scattering model, an adaptive luminance enhancement algorithm is proposed to make the image brighter and more prominent in detail after dehazing.

2. Dark channel priori theory

In the field of image dehazing, the atmospheric scattering model [13] plays a key role by modelling the process of haze image formation, i.e:

$$I(x) = J(x)t(x) + A(1-t(x)) \tag{1}$$

where $I(x)$ is the hazy image, $J(x)$ is the haze-free image, x denotes the pixel position in the image. A is the atmospheric light value and $t(x)$ is the

transmission map. $J(x)t(x)$ is the direct attenuation term and $A(1-t(x))$ is the atmospheric light imaging term.

For any image, the dark channel is defined:

$$J^{dark}(x)=\min_{y\in\Omega(x)}\left(\min_{c\in\{\mathrm{R,G,B}\}}J^{c}(\mathrm{y})\right) \tag{2}$$

where $J^{c}(\mathrm{y})$ is the color channel of any image, $\Omega(x)$ is a square local region centred at pixel point *x*. $J^{dark}(x)$ denotes the dark channel of this image, except for the sky region, $J^{dark}(x)\to 0$.

Assume that the atmospheric light value *A* is known and denoted by A^{c}, assume that the transmission map $t(x)$ is a constant and denoted by $\tilde{t}(x)$. Therefore, the transmission map equation is:

$$\tilde{t}(x)=1-\omega\min_{y\in\Omega(x)}\left(\min_{c}\frac{I^{c}(y)}{A^{c}}\right) \tag{3}$$

It has been shown that retaining some haze in the telephoto image can make the viewing effect better and more realistic. Therefore, an adjustment parameter $\omega(0<\omega<1)$ is introduced which can make the telephoto image retain some haze and is usually set to ω=0.95[14].

Furthermore, the final dehazing formula is obtained:

$$J^{c}(x)=\frac{I^{c}(x)-A^{c}}{max(\tilde{t}(x),t_{d})}+A^{c} \tag{4}$$

Since when $t(x)$ the value is taken close to zero, it results in an unnatural dehazed image, the minimum value of transmittance is t_{d} to be set as the threshold, so it is set to 0.1[15].

3. Our algorithm

The flow of our proposed image dehazing method is shown in Fig. 1.

Firstly, the luminance augmentation branch is executed, which performs CP-CLAHE processing and adaptive luminance augmentation processing on the input images respectively and fuses the two pre-processed images obtained with multiple weights. At the same time, the model optimization branch is executed, which uses the quadtree search algorithm and the gradient-domain guided filtering algorithm to optimize the atmospheric light value and transmittance in the atmospheric scattering model, respectively, and solves the dehazing image inversely. Finally, the images obtained from the two branches are fused and color-corrected to get a clear image.

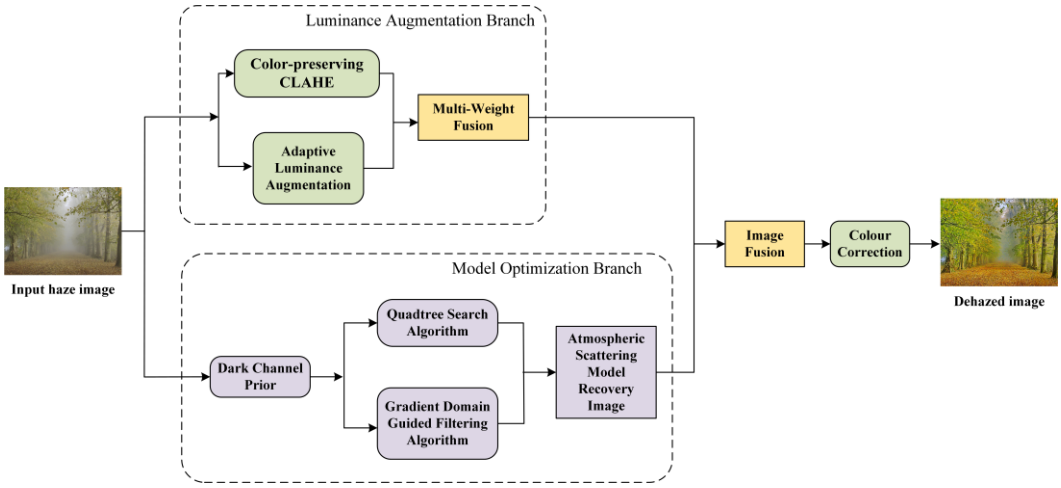

Fig. 1 Flowchart of the proposed method

3.1 Model optimization branch

The dark channel, a priori dehazing model is a classical method within the realm of image dehazing. However, the model is easily affected by image noise, which leads to errors in the estimated atmospheric light value and transmittance, which in turn affects the dehazing effect. Therefore, we propose an optimized version of the model to solve the above problems.

The dark channel a priori dehaze model usually picks the pixel points in the first 0.1% brightness and selects the point with the highest pixel value as the atmospheric light value. However, suppose bright lights appear in the haze image. In that case, the method will mistake the lights for haze regions, leading to the wrong selection of atmospheric light values and distorting the recovered image. Therefore, a hierarchical search strategy based on quadtree subdivision optimizes the selection of atmospheric light values.

First, the input image is divided equally into four subregions. Then, a resultant value is obtained by subtracting the standard deviation of the pixel values within the region from the average pixel value of each subregion. The subregion yielding the largest resultant value is chosen and further divided into four smaller subregions. After continuous iteration, when the size of the selected region is smaller than a pre-set threshold, the iteration is stopped, and the region is regarded as the selected range for the atmospheric light estimate. Finally, within this range, the color vector closest to the pure white light vector (255,255,255) is selected as the atmospheric light value A.

The dark channel dehazing model uses guided filtering to optimize the transmittance, but this method leads to halo artifacts in the processed image. Therefore, we first down sample the image in chunks using bilinear interpolation and then optimize the transmittance by introducing a gradient-domain guided filter [16]. Finally, we use up sampling to restore the image's original size. Unlike

the traditional guided filtering method, this can better preserve the edge structure and eliminate the edge-induced halo phenomenon.

The optimized atmospheric light values and transmittances were substituted within the final recovery equation:

$$J(x) = \frac{I(x) - A}{\max(t(x), t_0)} + A \tag{5}$$

3.2 Luminance augmentation branch

Although the model optimization branch can effectively remove the haze in the image, the image after dehazing will have problems with color distortion, dark brightness, and unclear details. To address the above problems, we adopt the method of image enhancement.

Inspired by the literature [4], we consider the cascading of RGB channels when performing CLAHE processing, and this operation allows the processed image to retain its original colors and enhance the image detail information.

Firstly, the color channels of the haze image I are reconstructed according to the method of literature [4], i.e:

$$I_{RT} = \mathrm{RT}(I) \tag{6}$$

where $\mathrm{RT}(\cdot)$ denotes the transformation.

Since the classical AHE algorithm leads to noise in the image while enhancing the details, in order to overcome this problem, we replace the AHE process with CLAHE, which avoids the introduction of excessive noise as compared to AHE. As a result, the CLAHE algorithm is applied to the image I_{RT}:

$$I_{C,RT} = \mathrm{CLAHE}(I_{RT}) \tag{7}$$

where $\mathrm{CLAHE}(\cdot)$ parameters take the default settings.

Finally, the enhanced result $I_{C,RT}$ is inversely reconstructed, i.e., converted back to RGB color space to obtain the processed image:

$$I_C = \mathrm{RT}^{-1}(I_{C,RT}) \tag{8}$$

To demonstrate that CP-CLAHE outperforms CP-AHE and is better suited for our method framework, we conducted focused ablation experiments on the benchmark dataset SOTS (Outdoor). For a comprehensive understanding of these experiments, please refer to Part IV of this paper.

While the CP-CLAHE algorithm enhances image contrast and refines details, it falls short in effectively addressing the issue of dark brightness. To tackle this challenge, we propose an adaptive luminance augmentation algorithm.

Direct processing of RGB images usually requires separate operations on R, G, and B channels, possibly leading to image color distortion. In contrast, the image brightness can be adjusted independently in HSV color space without affecting the colors, and the processed result is more in line with the human eye's

visual effect. Firstly, the image is converted from the original color space to the HSV color space. Secondly, it is assumed that the highest grey value of HSV in the image corresponds to the brightest point in the image, and the lowest grey value of HSV corresponds to the least bright point in the image. Following this assumption, the HSV image can be normalized and stretched using the following equation:

$$I_{\mathrm{HSV}}(x) = x_{\min} + (x - x_{\mathrm{low}}) \cdot \frac{x_{\max} - x_{\min}}{x_{\mathrm{high}} - x_{\mathrm{low}}} \tag{9}$$

where I_{HSV} is the processed HSV image, x_{high} and x_{low} are the value of the brightest pixel and the value of the darkest pixel in the current image, $x_{\max}$ and $x_{\min}$ are the maximum and minimum values of the image channel, $x_{\max} - x_{\min}$ =255.

Instead of simply using the brightest and darkest individual pixels, we set a set of thresholds as the lightest or darkest pixel values in the image. Next, this threshold is employed to limit the stretching of the HSV image, and the threshold can be expressed as:

$$\begin{cases} x'_{\mathrm{high}} = min\{x \mid I_v(x) \geq w_v n_v\} \\ x'_{\mathrm{low}} = max\{x \mid I_v(x) \leq w_v(1-n_v)\} \end{cases} \tag{10}$$

where x'_{high} and x'_{low} are the new brightest pixel value and darkest pixel value. I_v is the V channel of image I, w_v is the maximum pixel value of the current channel, and n_v is the quantization value of the set V channel.

Given that the original H channel values lie within the range of [0, 360], we employ a straightforward linear transformation to map these values onto the range of [0, 1], thereby ensuring consistency in the processing of the H (Hue) with that of the S(Saturation) and V(Value):

$$H' = \frac{H}{360} \tag{11}$$

For the calculation of the quantization factor *n*, the following formula can be used:

$$n = \frac{\bar{I}_{H'}(x) + \bar{I}_S(x) + \bar{I}_V(x)}{\bar{I}_V(x)} \tag{12}$$

where $\bar{I}_{H'}(x)$, $\bar{I}_S(x)$, $\bar{I}_V(x)$ is the average value of each channel of HSV.

Finally, to facilitate the display and saving of the image, then the HSV color space is converted back to the original color space.

Inspired by the literature [17] and considering that multi-weight fusion in the field of underwater image processing can effectively fuse two preprocessed images, we adopt Laplacian contrast weight, local contrast weight, saliency weight, saturation weight, and exposure weight to perform multi-weight fusion.

3.3 Image fusion

The images obtained from the above two branches can be fused to improve the accuracy and robustness of the dehazing and the structure and details of the fused images can be effectively preserved. Inspired by the literature [18], we first decompose each image into global and local components and then calculate the features of each component by constructing a pixel-level weight map.

In Fig. 2, (a) is the image after the model optimization branch processing, (b) is the image after the luminance augmentation branch processing, and (c) is the fused image, from which it can be seen that the fused image retains the clear and bright details of the input image 2 and also retains the dehazing effect of the input image 1. The dehazing effect of the fused image is improved while avoiding the loss of detailed information.

(a) (b) (c)

Fig. 2 Analysis of results

3.4 Color correction

After the above processing series, the fused image may have a problem with color deviation. To further improve the image quality, we introduce a color correction method based on SLVC [19] to solve the above problem. The method can also enhance the saturation of the dehazed image so that the colors of the processed image are brighter. The method involves directly processing pixels, removing biased colors by linearly stretching and transforming the pixels, and adjusting the contrast and saturation of the image by constructing competing relationships between data terms and regular terms. The literature [19] provides more details. SLVC as the last part of our algorithmic model has more robustness. Fig. 3 shows the final results of processing our algorithm. (a) is the input hazy image and (b) is the dehazed image. The processed image has higher contrast, saturation, and sharpness, presenting a more natural visual effect.

(a) (b)

Fig. 3 Results of our dehazing method

4. Experimental results and analysis

To validate the performance of our method, we selected both classical and novel dehazing methods for subjective and objective comparisons. Including one image enhancement-based method CEEF (Contrast enhancement and exposure fusion)(2022)[4], two image restoration-based methods IDE(Image dehazing and exposure)(2021)[7] and SLP(Saturation line prior)(2023)[8] and three deep learning based methods Dehaze-Net(An end-to-end system for single image haze removal)(2016)[9], MSBDN(Multi-scale boosted dehazing network)(2020)[10] and MADN(Meta-attention dehazing networks) (2022)[12]. We conducted comparisons using both subjective effects and objective evaluations to demonstrate the superiority of our method. Furthermore, ablation experiments were utilized to verify the effectiveness of each component within our method.

4.1 Datasets

Four datasets were used for the experimental data: 32 real scenes provided in the literature [4], 500 images of SOTS (outdoor) and 500 images of SOTS (indoor) provided in the public dataset RESIDE, and 1000 images randomly selected from the RTTS in RESIDE dataset, totalling 2032 images. The image format is PNG and the image sizes were experimented according to the sizes provided in the dataset without any changes.

4.2 Evaluation metrics

To objectively analyze the method performance, we choose the information entropy(IE) [20], the average gradient(AG) [21], the haze concentration index FADE [22], the peak signal-to-noise ratio(PSNR) [23] and the structural similarity index measurement system(SSIM) [24] for evaluating different dehazing methods.

4.3 Subjective evaluation

Figures 4 to 7 show the test results of different dehazing methods on the literature [4] test set, RTTS, SOTS (Indoor), and SOTS (Outdoor), respectively.

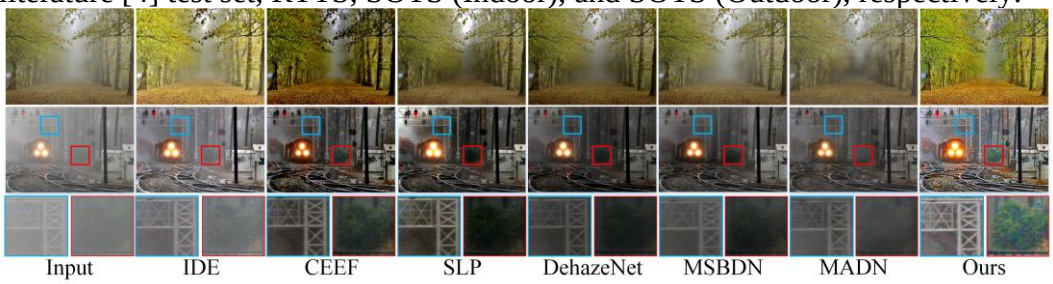

Fig. 4 Subjective comparison chart of literature [4] test set

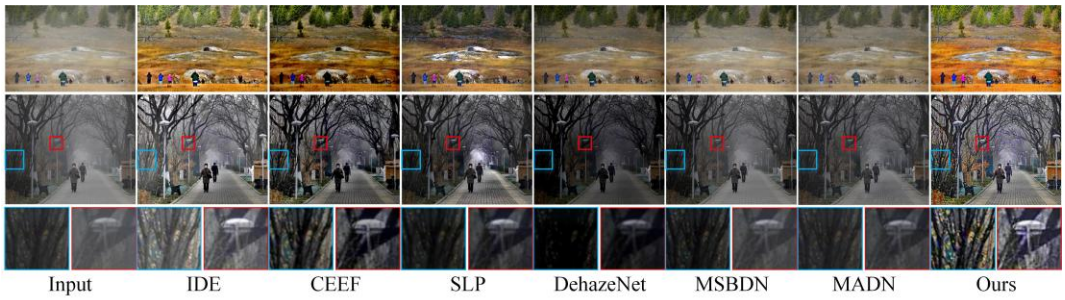

Fig. 5 Subjective comparison chart of RTTS

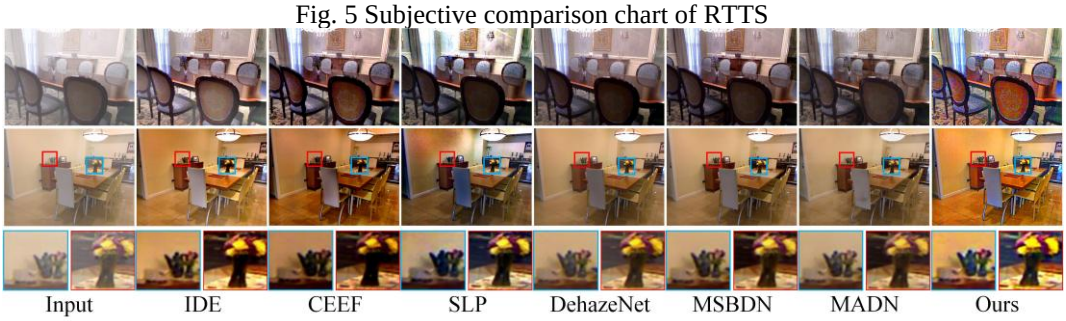

Fig. 6 Subjective comparison chart of SOTS(Indoor)

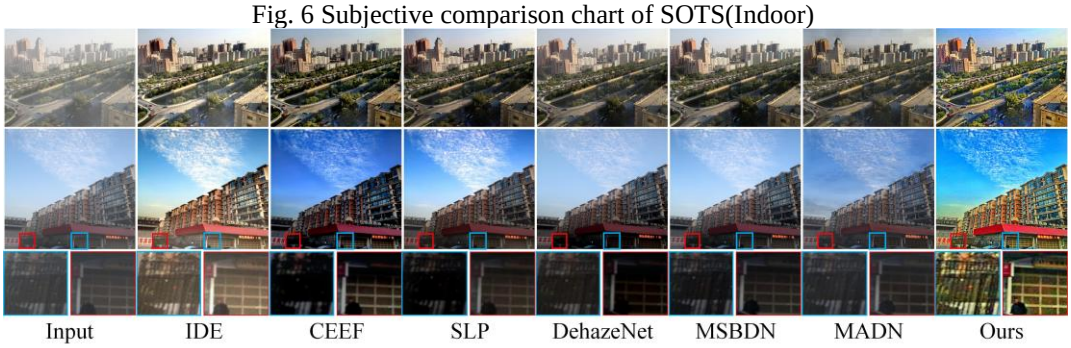

Fig. 7 Subjective comparison chart of SOTS(Outdoor)

From Fig. 4, it can be seen that our method can well restore the clarity of objects such as distant bushes and shelves without color distortion. As seen in Fig. 5, our method handles the detailed parts of the edges of the tree branches and street lamps very clearly, and the image's overall color is bright. As seen from Fig. 6, our method handles the bouquets with bright colors and the objects on the table with precise details. From Fig. 7, our method can recover the details of the door and window parts of the image well, and the colors of the sky region are natural and bright after processing. In summary, the visual effect of the processed image of our proposed method is significantly better than other methods.

4.4 Subjective evaluation

The data in Table 1 are the average of all image test results for each test set. The data in Table 2 are the average of all image test results within the SOTS (Outdoor) and SOTS (Indoor) datasets. Arrows pointing up signify higher and

better indicators, with optimal indicators denoted by bold fonts; in Table 1, sub-optimal indicators are underlined.

In Table 1, our proposed method achieves optimal average gradient scores across all test sets. Optimal values of information entropy were achieved on the RTTS, SOTS (Outdoor) and SOTS (Indoor) test sets and optimal FADE scores on SOTS (Outdoor) and SOTS (Indoor), with suboptimal FADE scores on RTTS and literature [4].

Table 1

Comparison of different methods

Datasets	Metrics	IDE	CEEF	SLP	DehazeNet	MSBDN	MADN	Ours
Literature [4]	IE ↑	**7.675**	6.950	7.311	7.311	7.444	7.191	7.611
	AG ↑	13.868	14.053	11.812	7.328	9.541	6.941	**19.237**
	FADE ↓	0.409	**0.208**	0.296	0.487	0.534	0.545	0.215
RTTS	IE ↑	7.637	7.054	7.491	7.188	7.419	7.223	**7.703**
	AG ↑	11.313	11.742	8.829	6.849	6.757	5.854	**17.209**
	FADE ↓	0.631	**0.277**	0.520	0.604	0.826	0.906	0.300
SOTS (Outdoor)	IE ↑	7.632	7.319	7.506	7.401	7.520	7.282	**7.784**
	AG ↑	11.985	12.562	9.123	7.304	8.464	6.987	**18.992**
	FADE ↓	0.570	0.282	0.508	0.622	0.726	0.685	**0.220**
SOTS (Indoor)	IE ↑	7.553	7.141	7.483	7.426	7.484	7.439	**7.699**
	AG ↑	5.962	7.205	5.875	4.533	5.304	4.512	**10.228**
	FADE ↓	0.646	0.313	0.479	0.677	0.499	0.659	**0.283**

Table 2

Comparison of PSNR and SSIM

Methods	SOTS(Outdoor)		SOTS(Indoor)	
	PSNR ↑	SSIM ↑	PSNR ↑	SSIM ↑
IDE	15.4847	0.8073	11.7191	0.4744
CEEF	16.3699	0.7997	12.5925	0.4718
SLP	**19.5250**	**0.8856**	13.0163	0.5440
DehazeNet	17.1243	0.5660	12.8600	0.5195
MSBDN	18.4670	0.6071	**13.2052**	**0.5555**
MADN	15.7855	0.5668	13.3376	0.5300
Ours	15.5015	0.7187	11.5005	0.3921

Table 2 shows that our method is not dominant in terms of PSNR and SSIM metrics. The reason for this is that our method tends to generate brighter and clearer dehazed images and to solve the problem of darker images after dehazing processing and the problem of incomplete dehazing, which is very different from the ground truth image. Moreover, the PSNR and SSIM metrics reflect part of the image reconstruction quality but may not fully represent the subjective perception of the human eye or the performance in real application

scenarios. In summary, our method performs better in terms of brightness, clarity and dehazing effect.

4.5 Ablation study

Eight ablation experiments were conducted on the SOTS (Outdoor) test set to validate each combination's effectiveness in our algorithmic framework.

1) BEOM represents the framework of our method.

2) w/o IM represents interchanging the positions of multi-weight fusion and image fusion in BEOM.

3) w/o II represents replacing multi-weight fusion with image fusion in BEOM.

4) w/o MM represents replacing image fusion with multi-weight fusion in BEOM.

5) w/o AHE represents replacing CP-CLAHE in BEOM with CP-AHE.

6) w/o DS represents removing SLVC in BEOM.

7) w/o DOM represents removing the model optimization branch in BEOM.

8) w/o DB represents removing adaptive brightness enhancement in BEOM.

9) w/o DC represents removing CP-CLAHE in BEOM.

Table 3 gives the objective evaluation results of the test set, with the optimal metrics in bold font. From this, it can be seen that our algorithmic framework achieved the highest IE, AG and FADE scores.

Table 3

Results of ablation experiments

Methods	IE ↑	AG ↑	FADE ↓
w/o IM	7.687	15.603	0.287
w/o II	7.648	18.147	0.244
w/o MM	7.710	15.334	0.294
w/o AHE	7.693	17.513	0.276
w/o DS	7.696	18.618	0.270
w/o DOM	7.773	18.777	0.283
w/o DB	7.617	18.562	0.245
w/o DC	7.686	16.463	0.314
BEOM	**7.784**	**18.992**	**0.220**

4.6 Runtime analysis

To analyze the running time of different methods, we test three different sizes of haze images, running MATLAB R2020a on Intel i5-8265U CPU and PyTorch based on NVIDIA RTX3090 on Ubuntu 20.04 system. The results of the experiments are shown in Table 4, and the results show that our proposed approach has poor real-time performance. However, there is little difference in

time between our method and the other compared methods when dealing with small-sized images. Also, based on the above subjective and objective performance, our method performs better regarding image quality improvement.

Table 4

Running time of different methods (unit: s)

Methods	Image size			Platform
	256×256	640×480	1024×768	
IDE	0.674	2.198	6.056	Matlab(CPU)
CEEF	0.667	1.131	2.551	Matlab(CPU)
SLP	0.831	3.161	7.594	Matlab(CPU)
DehazeNet	0.489	2.005	4.863	Matlab(CPU)&mex
MSBDN	0.127	0.421	1.413	PyTorch(GPU)
MADN	1.314	3.624	8.672	PyTorch(GPU)
Ours	1.614	4.473	10.578	Matlab(CPU)

4.7 Applications

To further evaluate the performance of our method on other low-visibility tasks, we randomly selected four images from the LOL low-light dataset [25] and the RSID remote sensing dataset [26] for processing. The results are shown in Fig. 8 and 9.

(a) Input image

(b) Output image

Fig. 8 Low-Light images enhancement

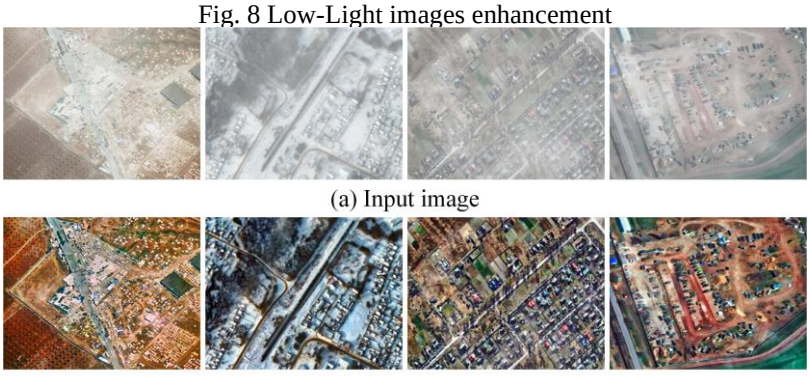

(a) Input image

(b) Output image

Fig. 9 Remote sensing images dehazing

As can be seen from the Fig. 8 and 9, without any parameter fine-tuning, our method achieves good processing effects on both low-light and remote sensing images, demonstrating broad application value in real-life scenarios.

5. Conclusions

Aiming at the existing dehazing model, which has the problems of poor dehazing effect, dark brightness, and color distortion after processing, a dehazing method based on model optimization and luminance augmentation is proposed. By comparing with the mainstream and the latest methods, the experimental results show that our method is effective in dehazing. Although our method is inferior to other comparative methods in terms of runtime and also suffers from the issue of unnatural appearance in the processed images, it demonstrates significant advantages in dehazing performance. The enhanced image clarity and color richness provide a advantage in practical applications, such as low-light enhancement and remote sensing. In these scenarios, the quality of the dehazed images is crucial for accurate object detection, scene understanding, and decision-making.

In future work, we plan to further optimize our method to enhance its operational efficiency and improve the naturalness of the processed images without compromising the dehazing performance.

REFERENCES

[1] *A. K. Shekar, L. Gou, L. Ren, et al.* Label-free robustness estimation of object detection CNNs for autonomous driving applications[J]. International Journal of Computer Vision, 2021, 129: 1185-1201.

[2] *K. Chi, Y. Yuan, Q. Wang.* Trinity-Net: Gradient-guided Swin transformer-based remote sensing image dehazing and beyond[J]. IEEE Transactions on Geoscience and Remote Sensing, 2023, 61: 1-14.

[3] *Z. Q. Zhao, P. Zheng, S. Xu, et al.* Object detection with deep learning: A review[J]. IEEE transactions on neural networks and learning systems, 2019, 30(11): 3212-3232.

[4] *X. Liu, H. Li, C. Zhu,* Joint contrast enhancement and exposure fusion for real-world image dehazing[J]. IEEE transactions on multimedia, 2022, 24: 3934-3946.

[5] *K. He, J. Sun, X. Tang,* Single image haze removal using dark channel prior[J]. IEEE transactions on pattern analysis and machine intelligence, 2010, 33(12): 2341-2353.

[6] *K. He, J. Sun, X. Tang,* Guided image filtering[J]. IEEE transactions on pattern analysis and machine intelligence, 2012, 35(6): 1397-1409.

[7] *M. Ju, C. Ding, W. Ren, et al,* IDE: Image dehazing and exposure using an enhanced atmospheric scattering model[J]. IEEE Transactions on Image Processing, 2021, 30: 2180-2192.

[8] *P. Ling, H. Chen, X. Tan, et al,* Single image dehazing using saturation line prior[J]. IEEE Transactions on Image Processing, 2023, 32: 3238-3253.

[9] *B. Cai, X. Xu, K. Jia, et al,* Dehazenet: An end-to-end system for single image haze removal[J]. IEEE transactions on image processing, 2016, 25(11): 5187-5198.

[10] *H. Dong, J. Pan, L. Xiang, et al,* Multi-scale boosted dehazing network with dense feature fusion[C]//Proceedings of the IEEE/CVF conference on computer vision and pattern recognition. 2020: 2157-2167.

[11] *T. Y. Jia, L. Zhuo, J. F. Li, et al,* Research advances on deep learning based single image dehazing [J]. Acta Electronica Sinica, 2023, 51(1): 231-245.

[12] *T. Jia, J. Li, L. Zhuo, et al,* Effective meta-attention dehazing networks for vision-based outdoor industrial systems[J]. IEEE Transactions on Industrial Informatics, 2022, 18(3): 1511-1520.

[13] *E. J. McCartney,* Optics of the atmosphere: scattering by molecules and particles[J]. New York, 1976.

[14] *X. Z. Sang, H. T. Zhu, H. Cheng, et al,* Fast image dehazing method based on dark channel and global estimation [J]. Progress in Lasers and Optoelectronics, 2022, 59(10): 121-129.

[15] *Y. Q. Liu, Z. W. Li, S. K. Yu, et al,* Shortwave infrared image dehazing based on dark channel prior [J]. Infrared Technology, 2023, 45(9): 954-961.

[16] *F. Kou, W. Chen, C. Wen, et al,* Gradient domain guided image filtering[J]. IEEE Transactions on Image Processing, 2015, 24(11): 4528-4539.

[17] *S. Wang, Z. Chen, H. Wang,* Multi-weight and multi-granularity fusion of underwater image enhancement[J]. Earth Science Informatics, 2022, 15(3): 1647-1657.

[18] *Z. Zhu, H. Wei, G. Hu, et al,* A novel fast single image dehazing algorithm based on artificial multiexposure image fusion[J]. IEEE Transactions on Instrumentation and Measurement, 2020, 70: 1-23.

[19] *J. Zhou, L. Pang, D. Zhang, et al,* Underwater image enhancement method via multi-interval subhistogram perspective equalization[J]. IEEE Journal of Oceanic Engineering, 2023, 48(2): 474-488.

[20] *R. Chan, M. Rottmann, and H. Gottschalk,* "Entropy maximization and meta classification for out-of-distribution detection in semantic segmentation," in 2021 IEEE/CVF International Conference on Computer Vision (ICCV), 2021, pp. 5108–5117.

[21] *R.S. Liu, L. Ma, J.A. Zhang, et al.* Retinex-inspired unrolling with cooperative prior architecture search for low-light image enhancement[C]//Proceedings of the IEEE/CVF conference on computer vision and pattern recognition. 2021: 10561-10570.

[22] *L. K. Choi, J. You, A. C. Bovik,* Referenceless prediction of perceptual fog density and perceptual image defogging[J]. IEEE Transactions on Image Processing, 2015, 24(11): 3888-3901.

[23] *I. Avcibas, B. Sankur, K. Sayood.* Statistical evaluation of image quality measures[J]. Journal of Electronic imaging, 2002, 11(2): 206-223.

[24] *Z. Wang, A. C. Bovik, H. R. Sheikh, et al.* Image quality assessment: from error visibility to structural similarity[J]. IEEE transactions on image processing, 2004, 13(4): 600-612.

[25] *C. Wei, W. Wang, W. Yang, et al.* Deep Retinex Decomposition for Low-Light Enhancement[J]. 2018.DOI:10.48550/arXiv.1808.04560.

[26] *K. Chi, Y. Yuan, Q. Wang.* Trinity-Net: Gradient-guided Swin transformer-based remote sensing image dehazing and beyond[J]. IEEE Transactions on Geoscience and Remote Sensing, 2023, 61: 1-14.